Consequences of Spin-Orbit Coupling at the Single Hole Level: Spin-Flip Tunneling and the Anisotropic g Factor

A. Bogan, S. A. Studenikin, M. Korkusinski, G. C. Aers, L. Gaudreau, P. Zawadzki, A. S. Sachrajda, L. A. Tracy, J. L. Reno, and T. W. Hargett

Phys. Rev. Lett. **118**, 167701 — Published 20 April 2017

DOI: 10.1103/PhysRevLett.118.167701

Consequences of spin-orbit coupling at the single hole level: spin-flip tunneling and anisotropic g-factor

A. Bogan, S. A. Studenikin,* M. Korkusinski, G. C. Aers, L. Gaudreau, P. Zawadzki, and A. S. Sachrajda†
Emerging Technology Division, National Research Council, Ottawa, Canada, K1A0R6

L. A. Tracy, J. L. Reno, and T. W. Hargett
Sandia National Laboratories, Albuquerque, New Mexico 87185, USA
(Dated: April 3, 2017)

Hole transport experiments were performed on a gated double quantum dot device defined in a p-GaAs/AlGaAs heterostructure with a single hole ocupancy in each dot. The charging diagram of the device was mapped out using charge detection confirming that the single hole limit is reached. In that limit, a detailed study of the two-hole spin system was performed using high bias magneto-transport spectroscopy. In contrast to electron systems, the hole spin was found not to be conserved during inter-dot resonant tunneling. This allows one to fully map out the two-hole energy spectrum as a function of the magnitude and the direction of the external magnetic field. The heavy-hole g-factor was extracted and shown to be strongly anisotropic, with a value of 1.45 for a perpendicular field and close to zero for an in-plane field as required for hybridizing schemes between spin and photonic quantum platforms.

Interest in quantum networks [1] and long-distance quantum cryptography [2, 3] led to proposals towards interfacing the photonic and solid-state spin qubits in gated lateral quantum dot devices [4, 5]. Such an interface is a central element in quantum sensors and quantum repeaters [6, 7], but could also be used to simplify the layout of multi-qubit gated devices [8]. An intermediate step in the transfer of the photon polarization state onto the state of the spin involves generation of an electron-hole pair. Therefore, beside long spin coherence time, the existing proposals [4, 6, 7] call for optical access (direct bandgap material) and engineering near-zero effective g-factor for the electron or the hole. While $g^* = 0$ is desired, in practice it should be small enough for the resulting Zeeman splitting to be smaller than the photon bandwidth [6, 7]. Currently the longest spin coherence times have been demonstrated for electron spin qubits in ^{28}Si[9], but their coupling to light is challenging due to the indirect bandgap. GaAs electronic devices, while more promising [4, 5], still require g-factor engineering.

In this Letter, we propose the heavy-hole spin confined in a gated GaAs double-dot device (DQD) as a candidate for the solid-state qubit in the photonic interface. We explore high-bias magneto-transport properties of a p-type AlGaAs/GaAs DQD [10]. Charge detection is used to tune the DQD to the two-hole regime, where certain tunneling transitions requiring spin flips are subject to Pauli spin blockade [11]. In our device this blockade is absent. This allows us to map out the energies of the two-hole quantum dot states with all spin projections as a function of magnetic field, and to extract the effective hole g-factor g^* as a function of the magnetic field tilt angle. We find that g^* exhibits a dramatic anisotropy, with a near-zero value for the in-plane field, thereby enabling the g-factor tuning *in situ*.

In consequence of the p-type character of the hole wavefunctions, the valence band includes heavy-hole (HH) and light-hole (LH) states. The hole properties are traced to the amount of HH-LH subband mixing [12, 13], which is related to the details of quantum confinement, strain, and the spin-orbit interaction. The early prediction of greatly reduced hyperfine interaction between hole and nuclear spins, and concomitant increased coherence times [14, 15], were confirmed experimentally in systems with small HH-LH mixing realized as self-assembled dots (SADs) [16–18] or nanowires [19]. In this regime the strong anisotropy of the hole g-factor is expected [12]. To date, however, only partial anisotropy was demonstrated, e.g., in InAs SADs [20] and silicon nanowires [21]. Holes in GaAs are also subject to strong Dreselhaus and Rashba spin-orbit interactions, which introduce the coherent spin-flip tunneling [12, 13]. In silicon DQDs these interactions are absent, leading to Pauli spin blockade [21–23]. On the other hand, early experiments on GaAs DQDs in many-hole regime show the spin-orbit-induced spin-flip transport [25]. In addition, our device provides a lateral confinement for the HH subband only, while the LH orbitals remain extended across the sample volume. In contrast to the SADs, where the LH subband remains confined [24], this property further decreases the HH-LH mixing.

Figure 1(a) shows a scanning electron micrograph of the DQD gate layout [26]. As shown by results of electrostatic simulations (Fig. 1(b)), for judiciously chosen gate voltages this layout creates a potential profile at the AlGaAs/GaAs heterointerface with two ellipsoidal minima. In Fig. 1(c) we plot the charging diagram, showing the derivative $\mathrm{d}I_{SC}/\mathrm{d}V_L$ of the charge sensor current I_{SC} over the L-gate voltage V_L, as a function of gate voltages V_L and V_R. It reveals the charge stability regions of configurations with different number (n_L, n_R) of holes in each QD. The (0,0) state was confirmed using techniques

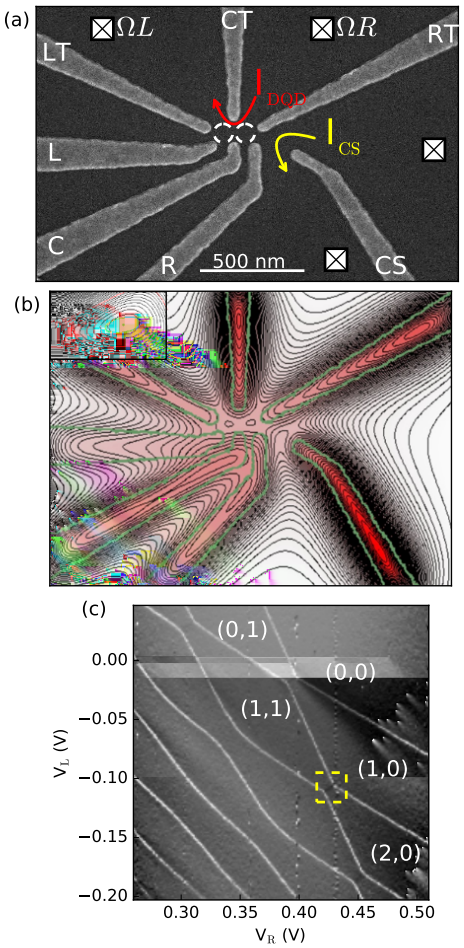

FIG. 1. (a) Scanning electron micrograph of the gate layout of the double dot device. Red (yellow) arrow indicates the transport (charge detection) current path. (b) Simulated potential profile created by gates at the level of the AlGaAs/GaAs heterointerface. The gate voltages have been adjusted to admit one hole in each dot from the two-dimensional hole gas. Inset: closeup on the potential of the right-hand dot. The contour line spacings are 769 μeV in the main graph and 25 μeV in the inset. (c) Charging diagram obtained by charge detection as a function of the voltages on the left (L) and right (R) gates. Square marks the region close to tunnel resonance between (1,1) and (2,0) configurations.

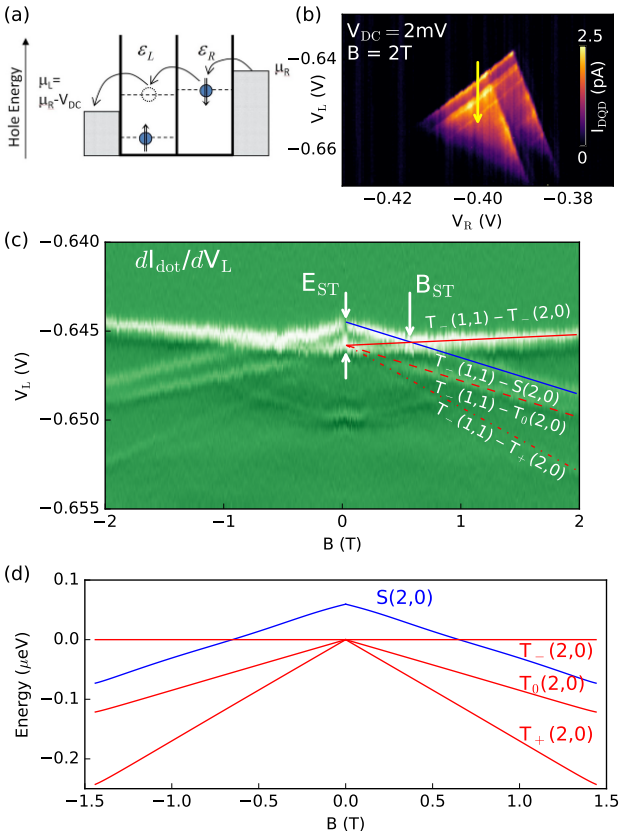

FIG. 2. (a) Schematic diagram of the high source-drain bias magneto-transport measurement. (b) The magneto-transport triangles at source-drain voltage V_{SD} = 2 mV mapped as a function of the voltages on the left (vertical axis) and right gate (horizontal axis) at a fixed magnetic field of 2T perpendicular to the sample. The upper triangle corresponds to the (1,0)→(1,1)→(2,0)→(1,0) tunneling sequence, while the lower one corresponds to the (2,0)→(2,1)→(1,1)→(2,0) sequence. (c) Derivative of the tunneling current as a function of the voltage V_L and the magnetic field, measured at millikelvin temperatures. The yellow arrow in (b) shows the gate voltage sweep trajectory. (d) Theoretically derived energy spectrum of the (2,0) system. The energies are measured from the energy of the state $T_-(2,0)$ (two holes spin-down in the left-hand dot).

similar to those used for few-electron QDs [27]. We focus on the region around the (1,1)–(2,0) charge transfer line where the Pauli spin blockade is commonly observed in electron DQDs. Results similar to this region were obtained at the equivalent (1,1)–(0,2) charge transfer line.

Figure 2(a) shows a schematic energy diagram of our high source-drain bias magneto-transport measurement. The tunneling follows the scheme (1,0)→(1,1)→(2,0)→(1,0). In DQDs confining electrons, this sequence is commonly used to reveal the Pauli spin blockade mechanism. At low magnetic fields, the lowest-energy state of the electronic (2,0) configuration is a spin singlet $S(2,0)$, while the $T(2,0)$ triplet manifold lies much higher in energy. The (1,1) configuration, prepared by tunneling, can be a singlet or a triplet. If it is a triplet $T(1,1)$, the transport will be blockaded. The blockade can be lifted at low magnetic fields by mixing of singlet and triplet states by the hyperfine interaction. The T(2,0) state can enter the transport window, providing a non-blockaded tunneling path for $T(1,1)$, only at large bias voltage and detuning [11].

Our hole device is different from the electronic system in two aspects. First, the HH in III-V materials experiences a strong spin-orbit interaction, causing the hole spin to rotate during tunneling [12, 13, 26]. In electronic devices this process was found to be orders of magnitude

weaker [28]. One expects, therefore, that the Pauli blockade will be lifted for all (1,1)→(2,0) tunneling channels. Second, the energy gap between the S(2,0) and T(2,0) states is much smaller than in electron dots due to the large hole mass. This allows one to map out the energies of the doubly-occupied singlet and triplets on equal footing.

Figure 2(b) shows the transport triangles obtained by applying a high DC bias (2 mV) across the device in the (1,1)–(2,0) regime at a magnetic field $B = 2$T. We observe two transport triangles, one corresponding to the above tunneling sequence, while the other one corresponds to the (2,1)→(1,1)→(2,0)→(2,1) sequence involving an additional hole. The resonant features in both triangles coincide, as in both cases the current is limited by the tunnel resonances between the (1,1) and (2,0) configurations. Inside the triangle one observes a series of lines marking high-amplitude tunneling current. These lines occur whenever the energy of the ground or excited state of the (2,0) configuration matches an energy level of the (1,1) configuration.

Figure 2(c) shows the derivative of the tunneling current with respect to the left gate voltage V_L as a function of the magnetic field. The sweeping trajectory of the V_L voltage is indicated in Fig. 2(b) by the yellow arrow. The observed lines can be understood as resonances between (2,0) and (1,1) states split by magnetic field. The intensity of lines depend on how many Zeeman-split levels are in resonance and whether spin-flip tunneling process is involved. The strongest line (red solid line) corresponds to three simultaneous resonances: $T_+(1,1)$ with $T_+(2,0)$, $T_0(1,1)$ with $T_0(2,0)$, and $T_-(1,1)$ with $T_-(2,0)$. The second strongest line (red dashed) involves one spin flip and two resonances, $T_-(1,1)$ with $T_0(2,0)$ and $T_0(1,1)$ with $T_+(2,0)$. Finally, the weakest line (red dot-dashed) marks one resonance of $T_-(1,1)$ with $T_+(2,0)$. The magneto-resonance spectra can be understood qualitatively, assuming that the spectroscopy of the left dot state is performed using the lowest-energy polarized hole triplet $T_-(1,1)$. This is the ground state of the (1,1) system at any finite magnetic field for which the Zeeman energy of two holes exceeds any correlation corrections, favouring the singlet ground state of the (1,1) charge configuration. For electrons this condition is already satisfied at millitesla fields; we expect that for holes the critical fields are even smaller due to the larger effective g-factor. As the voltage V_L is made more negative, the (2,0) configurations are shifted down in energy relative to $T_-(1,1)$. In Fig. 2(c) we are, therefore, mapping out the inverted energy spectrum of the left dot confining two holes.

Neglecting the diamagnetic shifts and the dependence of the spin-orbit and Coulomb hole-hole interactions on the magnetic field, we write the $T_-(1,1)$ energy as $E_{1,1} = E_{1,1}(B=0) - \bar{g}^*\mu_B B$, where $\bar{g}^*$ is the effective hole g-factor averaged between the two dots. In the (2,0) configuration, the singlet state involves two holes on the lowest single-particle orbital. Its energy $E^S_{2,0}$ is not renormalized by the Zeeman term. Next in energy is the triplet manifold. If we denote the triplet energy at zero magnetic field as $E^T_{2,0}$, the energies of the two polarized triplets $T_\pm(2,0)$ are $E^{T\pm}_{2,0}(B) = E^T_{2,0} \pm g^*\mu_B B$, respectively, while that of the unpolarized triplet $T_0(2,0)$ is $E^{T0}_{2,0}(B) = E^T_{2,0}$. Here g^* is the effective hole g-factor in the left-hand dot. Since all these energies depend on the magnetic field differently, the maxima corresponding to the resonances of $E_{1,1}$ with the (2,0) states will form linear features at different angles, as seen in Fig. 2(c). The resonance between $E_{1,1}$ and $E^S_{2,0}$ (blue) requires more negative voltage V_L with the increasing field, compensating for the Zeeman shift of the (1,1) state. The resonance with the $T_-(2,0)$ state (solid red line) evolves almost horizontally with the field, as energies of both $T_-(2,0)$ and $T_-(1,1)$ are affected identically by the Zeeman term. The resonance with $T_0(2,0)$ (dashed red) evolves approximately parallel to the resonance with $S(2,0)$ (blue); the slight difference in angle corresponds to different diamagnetic corrections to the energies of the two states. Lastly, the resonance with $T_+(2,0)$ (dot-dash red) evolves at the largest angle, as the energy difference between it and $T_-(1,1)$ is twice the Zeeman energy. Remarkably, this tunneling resonance involves two hole spin flips. We note that the high source-drain voltage allows to assign the spin projection to all (2,0) states unambiguously based on the slopes of the observed linear features. The direct resonant tunnel coupling of $T_-(1,1)$ to *all* (2,0) states is a clear evidence of the spin-orbit mediated spin-flip transport in agreement with theory [12, 26].

This magneto-transport spectrum is characterized by the singlet-triplet splitting at zero magnetic field $E_{ST} = 60$ μeV, and the magnetic field corresponding to the (2,0) singlet-triplet transition $B_{ST} = 0.65$ T (arrows in Fig. 2(c)). Using the single-particle spectrum calculated numerically [26] from potential profiles in Fig. 1(b), we obtain $E_{ST} = 285$ μeV and $B_{ST} = 2.15$T. We account for hole-hole interactions by renormalizing the singlet energy by a correction V_S, and each of the triplets by V_T. Typically $V_T < V_S$ [29], i.e., the interactions decrease both E_{ST} and B_{ST}. Parametrizing an approximate magnetic field dependence $V_{ST} = V_T - V_S = -V_0\left(1 + \sum_{k=1}^{4}\zeta_k B^k\right)$ (Refs. [26, 29]) we find $V_0 = 225$ μeV, $\zeta_1 = -0.05$ T^{-1}, $\zeta_2 = -1.13$ T^{-2}, $\zeta_3 = +0.92$ T^{-3}, and $\zeta_4 = -0.22$ T^{-4} by fitting simultaneously E_{ST} and B_{ST}. In Fig. 2(d) we plot the results of the theoretical calculation.

Figure 3(a) shows the tunneling current (not its derivative) extended over a wider range of perpendicular magnetic field. This set of measurements was performed in the ^{3}He setup which allowed us to tilt the magnetic field relative to the sample. Figure 3(b) shows a line graph through the panel (a) at $B = 2.95$ T. The current is dominated by the resonances and drops to very low val-

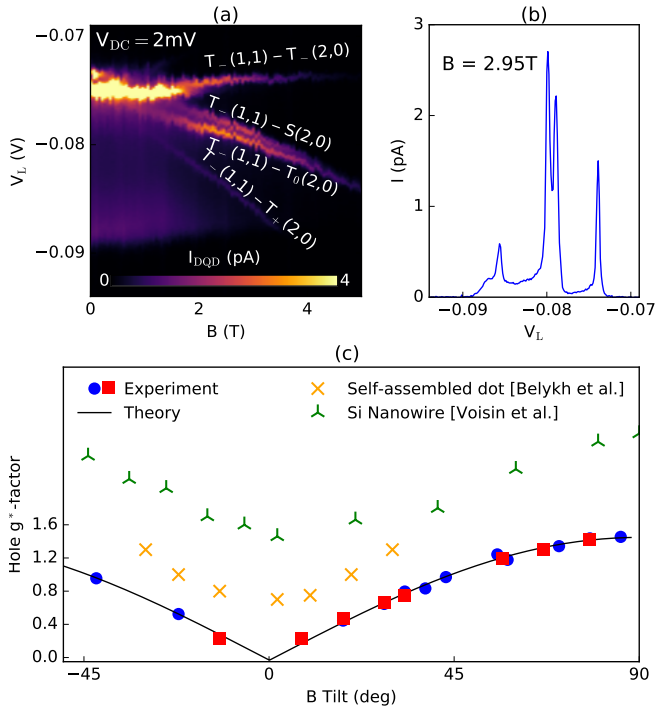

FIG. 3. (a) Magneto-transport measurement in the ^{3}He system as a function of the left gate voltage and the magnetic field; the measurement protocol is equivalent to that in Figs. 2(c,d). (b) A vertical line graph of (a) taken at $B = 2.95$ T. (c) Effective hole g-factor extracted from the magneto-transport spectra as a function of the tilt angle of the magnetic field with respect to the plane of the sample; the angle of 90 degrees corresponds to the field perpendicular to the sample plane. Red and blue symbols are measured values, while the black solid line is a fit to the relation $g^*(\theta) = g^*_\perp |\sin\theta| + g_{min}$ with $g^*_\perp = 1.45$ and $g_{min} = -0.04$. Orange (green) symbols mark hole g-factor in InAs SADs, Ref. [20] (Si nanowires, Ref. [21]).

ues between them. As in Fig. 2(c), we identify the resonant lines as resulting from the energy resonances of the $T_-(1,1)$ state with the four lowest two-hole (2,0) states. For any magnetic field, the energy gap $\Delta E(B)$ between the consecutive triplet traces is equal to the effective Zeeman energy. By translating the corresponding voltage through the lever arm values for our sample, we extract the effective hole g-factor $g^*_\perp = \Delta E(B)/\mu_B B = 1.45 \pm 0.1$ for the left-hand (doubly-occupied) dot. This value is consistent with Wang *et al.* [30]. We repeated the experiment using the transition (1,1)→(0,2) with the opposite source-drain voltage and obtained the same $g^*_\perp$ for the right-hand dot.

We next turn to study the g-factor anisotropy. Figure 3(c) shows results extracted from magneto-transport spectra as a function of the tilt angle θ of the magnetic field direction relative to the plane of the sample ($\theta = 90°$ is the perpendicular arrangement). The two series of symbols correspond to two independent measurements taken months apart on different cooldowns. In the HH limit [26] we expect the g-factor anisotropy in the form $g^*(\theta) = g^*_\perp |\sin\theta|$ with the in-plane g-factor $g_{min} = g^*(0) = 0$ (black line). We find an excellent agreement, with $g_{min} = -0.04 \pm 0.04$ obtained by fitting, as the overlapping transport peaks make the direct measurement at $\theta \approx 0$ difficult. This large g-factor anisotropy as a function of tilt, observed here for the first time in lateral gated devices, is related to the details of confinement of HH and LH states. Both hole subbands are confined vertically at the heterointerface. However, due to the disparity of the HH and LH effective masses along z-direction, only HHs are confined laterally by the gate potentials, while LHs form states propagating in-plane [26], which suppresses the HH-LH mixing. In Fig. 3(c) we set the dramatic anisotropy demonstrated in our experiment against the measurements in SADs [20] and silicon nanowire hole QDs [21], where the LH subband is confined, and in consequence the hole g-factor does not reach zero for in-plane magnetic field.

In summary, we presented magneto-transport studies of the lateral gated GaAs DQD in the two-hole regime. We find that the strong spin-orbit interaction enables strong resonant spin-flip hole tunneling between dots, a property of interest for fast coherent spin manipulations. This channel lifts the usual Pauli blockade mechanism and enables mapping out of the energies of states with different spin as a function of detuning and magnetic field. We find that the holes confined by our device are of HH character, with a strongly anisotropic g-factor, varying from $g^* = 1.45$ to zero for the field orientation varied from perpendicular to in-plane direction relative to the sample. These results suggest that hole devices are indeed promising for coherent photon to spin conversion schemes where a zero g-factor is required to prevent incidental which-path information [6]. Measurements are in progress to obtain the coherence time for single hole spins, which is expected to be greatly enhanced over the electron case.

Acknowledgment. BA and SS thanks The Natural Sciences and Engineering Research Council of Canada for financial support. This work was performed at the Center for Integrated Nanotechnologies, a U.S. DOE, Office of Basic Energy Sciences user facility, and Sandia National Laboratories, a multi-program laboratory operated by Sandia Corporation, a wholly owned subsidiary Lockheed-Martin Company, for the U. S. Department of Energy's National Nuclear Security Administration under Contract No. DE-AC04-94AL85000.

* Corresponding author, email: sergei.studenikin@nrc.ca
† Corresponding author, email: andy.sachrajda@nrc.ca

[1] H. J. Kimble, Nature **453,** 1023 (2008).

[2] L. M. Duan, M. D. Lukin, J. I. Cirrac, and P. Zoller, Nature **414,** 413 (2001).

[3] L. Childress, J. M. Taylor, A. S. Sorensen, and M. D. Lukin, Phys. Rev. Lett. **96,** 070504 (2005).

[4] A. Oiwa, T. Fujita, H. Kiyama, G. Allison, A. Ludwig, A. D. Wieck, and S. Tarucha, J. Phys. Soc. Japan **86,** 011008 (2017).

[5] K. Morimoto, T. Fujita, G. Allison, S. Teraoka, M. Larsson, H. Kiyama, S. Haffouz, D. G. Austing, A. Ludwig, A. D. Wieck, A. Oiwa, and S. Tarucha, Phys. Rev. B **90,** 085306 (2014).

[6] E. Yablonovitch, H. W. Jiang, H. Kosaka, H. D. Robinson, D. S. Rao, and T. Szkopek, Proc. IEEE **91,** 761 (2003).

[7] H. Kosaka, J. Appl. Phys. **109**, 102414 (2011).

[8] M. D. Shulman, O. E. Dial, S. P. Harvey, H. Bluhm, V. Umansky, and A. Yacoby, Science **336,** 202 (2012).

[9] A. M. Tyryshkin, S. Tojo, J. J. L. Morton, H. Riemann, N. V. Abrosimov, P. Becker, H.-J. Pohl, T. Schenkel, M. L. W. Thewalt, K. M. Itoh, and S. A. Lyon, Nature Materials **11,** 143 (2012).

[10] L. A. Tracy, T. W. Hargett, and J. L. Reno, Appl. Phys. Lett. **104,** 123101 (2014).

[11] K. Ono, D. G. Austing, Y Tokura, and S. Tarucha, Science **297,** 1313 (2002).

[12] D. V. Bulaev and D. Loss, Phys. Rev. Lett. **95,** 076805 (2005).

[13] P. Szumniak, S. Bednarek, B. Partoens, and F. M. Peeters, Phys. Rev. Lett. **109,** 107201 (2012).

[14] J. Fischer, W. A. Coish, D. V. Bulaev, and D. Loss, Phys. Rev. B **78,** 155329 (2008).

[15] J. Fischer and D. Loss, Phys. Rev. Lett. **105,** 266603 (2010).

[16] E. A. Chekhovich, A. B. Krysa, M. S. Skolnick, and A. I. Tartakovskii, Phys. Rev. Lett. **106,** 027402 (2011).

[17] B. D. Gerardot, D. Brunner, P. A. Dalgarno, P. hberg, S. Seidl, M. Kroner, K. Karrai, N. G. Stoltz, P. M. Petroff, and R. J. Warburton, Nature **451,** 441 (2008).

[18] S. G. Carter, S. E. Economou, A. Greilich, E. Barnes, T. Sweeney, A. S. Bracker, and D. Gammon, Phys. Rev. B **89,** 075316 (2014).

[19] V. S. Pribiag, S. Nadj-Perge, S. M. Frolov, J. W. G. van den Berg, I. van Weperen, S. R. Plissard, E. P. A. M. Bakkers, and L. P. Kouwenhoven, Nature Nanotechnol. **8,** 170 (2013).

[20] V. V. Belykh, D. R. Yakovlev, J. J. Schindler, E. A. Zhukov, M. A. Semina, M. Yacob, J. P. Reithmaier, M Benyoucef, and M. Bayer, Phys. Rev. B **93,** 125302 (2016).

[21] B. Voisin, R. Maurand, S. Barraud, M. Vinet, X. Jehl, M. Sanquer, J. Renard, and S. De. Franceschi, Nano Lett. **16,** 88 (2016).

[22] R. Li, F. E. Hudson, A. S. Dzurak, and A. R. Hamilton, Nano Lett. **15,** 7314 (2015).

[23] R. Maurand, X. Jehl, D. Kotekar Patil, A. Corna, H. Bohuslavskyi, R. Lavieville, L. Hutin, S. Barraud, M. Vinet, M. Sanquer, and S. De Franceschi, arXiv.org/1605.07599 (2016).

[24] P. Hawrylak and M. Korkusinski, *Electronic and optical properties of self-assembled quantum dots,* in: *Single Quantum Dots: Fundamentals, Applications, and New Concepts,* P. Michler (Ed.), Topics in Applied Physics **90,** 25 (Springer, Berlin, 2003).

[25] D. Q. Wang, O. Klochan, J.-T. Hung, D. Culcer, I. Farrer, D. A. Ritchie, and A. R. Hamilton, Nano Lett. **16,** 7685 (2016).

[26] See supplemental material, which includes Refs. [31 - 35].

[27] M. Ciorga, A. S. Sachrajda, P. Hawrylak, C. Gould, P. Zawadzki, S. Jullian, Y. Feng, and Z. Wasilewski, Phys. Rev. B **61,** R16315 (2000).

[28] T. Fujita, P. Stano, G. Allison, K. Morimoto, Y. Sato, M. Larsson, J.-H. Park, A. Ludwig, A. D. Wieck, A. Oiwa, and S. Tarucha, arXiv.org/1603.04861 (2016).

[29] J. Kyriakidis, M. Pioro-Ladriere, M. Ciorga, A. S. Sachrajda, and P. Hawrylak Phys. Rev. B **66,** 035320 (2002).

[30] D. Q. Wang, A. R. Hamilton, I. Farrer, D. A. Ritchie, and O. Klochan, Nanotechnology **27,** 334001 (2016).

[31] Y. Komijani, T. Choi, F. Nichele, K. Ensslin, T. Ihn, D. Reuter, and A. D. Wieck, Phys. Rev. B **88,** 035417 (2013).

[32] L. A. Tracy, J. L. Reno, and T. W. Hargett, LANL Report (2015).

[33] S. I. Dorozhkin, Solid State Commun. **72,** 211-214 (1989).

[34] R. Winkler, S. J. Papadakis, E. P. De Poortere, and M. Shayegan, Phys. Rev. Lett. **85,** 4574 (2000).

[35] M. Florescu and P. Hawrylak, Phys. Rev. B **73,** 045304 (2006).